JTTEE5 19:248–254
DOI: 10.1007/s11666-009-9434-y
1059-9630/$19.00 © ASM International

Modeling the Influence of Injection Modes on the Evolution of Solution Sprays in a Plasma Jet

Y. Shan, T.W. Coyle, and J. Mostaghimi

(Submitted April 24, 2009; in revised form September 17, 2009)

Solution precursor plasma spraying (SPPS) is a novel technology with great potential for depositing finely structured ceramic coatings with nano- and sub-micrometric features. The solution is injected into the plasma jet either as a liquid stream or gas atomized droplets. Solution droplets or the stream interact with the plasma jet and break up into fine droplets. The solvent vaporizes very fast as the droplets travel downstream. Solid particles are finally formed, and the particle are heated up and accelerated to the substrate to generate the coating. The deposition process and the properties of coatings obtained are extremely sensitive to the process parameters, such as torch operating conditions, injection modes, injection parameters, and substrate temperatures. This article numerically investigates the effect of injection modes, a liquid stream injection and a gas-blast injection, on the size distribution of injected droplets. The particle/droplet size, temperature, and position distributions on the substrate are predicted for different injection modes.

Keywords injection modes, modeling, solution plasma spraying, spray parameters

1. Introduction

Solution precursor plasma spraying (SPPS) is a novel technology with great potential for depositing finely structured ceramic coatings with nano- and sub-micrometric features (Ref 1-3). In this process, solutions of ceramic or metallic salts instead of ceramic or metallic powders are injected into the plasma jet either as a liquid stream or gas atomized droplets. Solution droplets or the stream interact with the plasma jet and break up into fine droplets. The solvent vaporizes very fast as the droplets travel downstream followed by precipitation and pyrolysis. Depending on the heating and trajectory history of droplets, different states of particles, (melted particles, small sintered particles, dry agglomerates, wet agglomerates, and wet droplets) (Ref 4), are formed and impact on the substrate to generate coatings. Studies have been carried out to understand the transport phenomena and the heating and trajectory of solution droplets (Ref 5-7), droplet breakup and collisions (Ref 6-8), coating deposition mechanism (Ref 4, 9), and characterization (Ref 1-3, 10, 11). The injection mode is one of the important factors that influence the injection and the heating and trajectory history of solution droplets. This article numerically investigates the effect of injection modes, a liquid stream injection and a gas-blast injection, on the size distribution of injected droplets. The temperature and flow fields of the Ar-H_2 plasma jet issuing into air are predicted by a three-dimensional (3D), time-dependent model with the RNG-based k-ε model to simulate the turbulence of the jet. The particle/droplet size, temperature, and position distributions on the substrate are predicted for different injection modes. The performance of different injection modes are analyzed based on the model predictions.

This article is an invited paper selected from presentations at the 2009 International Thermal Spray Conference and has been expanded from the original presentation. It is simultaneously published in *Expanding Thermal Spray Performance to New Markets and Applications: Proceedings of the 2009 International Thermal Spray Conference*, Las Vegas, Nevada, USA, May 4-7, 2009, Basil R. Marple, Margaret M. Hyland, Yuk-Chiu Lau, Chang-Jiu Li, Rogerio S. Lima, and Ghislain Montavon, Ed., ASM International, Materials Park, OH, 2009.

Y. Shan, College of Energy and Power Engineering, University of Shanghai for Science and Technology, Shanghai 200093, China; and **T.W. Coyle** and **J. Mostaghimi**, Centre for Advanced Coating Technology, University of Toronto, Toronto, ON, Canada. Contact e-mail: y.shan@utoronto.ca.

2. Mathematical Models

2.1 Plasma Jet and Droplets Behavior

The 3D model of the plasma jet (Fig. 1) is based on the following assumptions: (1) the flow is time dependent, incompressible, and turbulent with temperature-dependent properties; (2) the plasma is in local thermodynamic equilibrium and optically thin; (3) the arc voltage fluctuation is not considered; and (4) the solution is introduced radially into the jet. The governing equations of the model

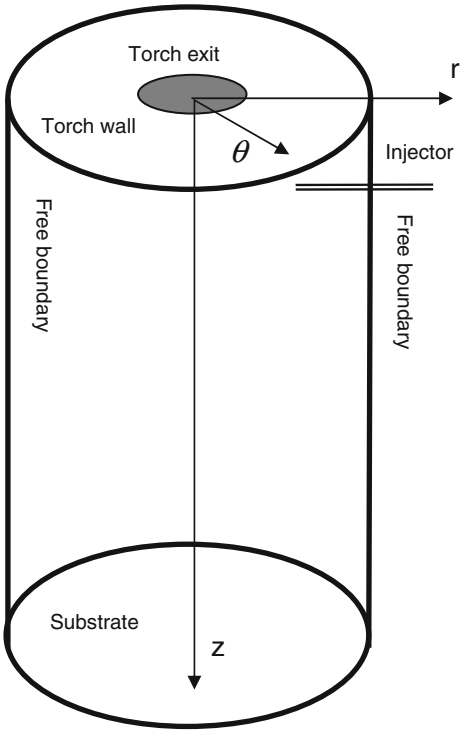

Fig. 1 3D computational domain

are the time-dependent conservation equations of mass, momentum, energy, and species.

$$\frac{D\rho}{Dt} + \rho\nabla\cdot\vec{u} = S_C^s \qquad \text{(Eq 1)}$$

$$\rho\frac{D\vec{u}}{Dt} = -\nabla P + \nabla\cdot\Gamma_\mu\nabla\vec{u} + \vec{S}_M^s \qquad \text{(Eq 2)}$$

$$\rho\frac{Dh}{Dt} = \nabla\cdot\Gamma_h\nabla h - Q_R + S_E^s \qquad \text{(Eq 3)}$$

$$\rho\frac{DY}{Dt} = \nabla\cdot\Gamma_D\nabla Y + S_C^s \qquad \text{(Eq 4)}$$

ρ is the gas density, t is time, P is pressure, h is the enthalpy, $\vec{u}$ is the velocity vector, Y is the mass fraction, Q_R is the radiation loss, and S_C^s, $\vec{S}_M^s$, and S_E^s, are the contributions of the solution spray to the equation of mass, momentum, and energy, respectively. Temperature-dependent transport and thermodynamic properties of plasma gases and air at atmospheric pressure are used. The mixing rule is adopted to take into account the effect of the mixing of solvent vapor on the properties of the jet. The turbulent kinetic energy and its dissipation are modeled using RNG-based k-ε model (Ref 5). It has to be noted that the arc voltage fluctuation is neglected here. According to recent studies (Ref 12, 13), however, the droplet injection, breakup, and dispersion may be affected by the variation of the momentum density of the jet caused by the arc voltage fluctuation. This should be included in the model in future study.

At the exit of the torch, the temperature and velocity are assumed to be given by

$$v = 0, \quad w = 0, \quad \text{and} \quad u = u_m\left(1 - \left(\frac{r}{R}\right)^m\right) \qquad \text{(Eq 5)}$$

$$T = (T_m - T_w)\left(1 - \left(\frac{r}{R}\right)^n\right) + T_w \qquad \text{(Eq 6)}$$

where T_m and u_m are maximum temperature and velocity at the gun exit, respectively, m and n are set to 2.6 and 7.8, respectively. They were determined from global mass and total enthalpy conservation (Ref 5).

To simulate the trajectories and heating of the solution droplets, the following assumptions are employed in this article: (1) the solution droplet is spherically symmetric; (2) the temperature within the solution droplet is assumed to be uniform; (3) the radiation from the droplet and the rarefaction effect are neglected; and (4) the aerodynamic drag force, thermophoretic force, and gravitational force are considered. Lagrangian equations of motion and heat and mass transfer are used to simulate the droplet behavior in the jet.

The velocity of a droplet can be calculated from the force balance on the droplet

$$\frac{du_d}{dt} = F_D(u - u_d) + \frac{g_x(\rho_d - \rho)}{\rho_d} + F_x, \qquad \text{(Eq 7)}$$

where $F_D(u - u_d)$ is the drag force per unit droplet mass, $F_D = \frac{18\mu}{\rho_d d_d^2}\frac{C_D Re}{24}$ $(0.1 \le Re \le 5.0 \times 10^4)$. F_x is the thermophoretic force. The drag coefficient is calculated by the correlation of Morsi and Alexander (Ref 14).

During the first stage of the heating of an individual solution droplet, no mass transfer occurs. The droplet temperature is calculated by heat balance equation neglecting the radiation from the droplet as follows

$$m_d c_d\frac{dT_d}{dt} = h_d A_d(T_f - T_d). \qquad \text{(Eq 8)}$$

After the droplet temperature reaches its vaporization temperature, the rate of vaporization is governed by gradient diffusion. The droplet temperature is determined by

$$m_d c_d\frac{dT_d}{dt} = h_d A_d(T_f - T_d) + \frac{dm_d}{dt}h_{fg}. \qquad \text{(Eq 9)}$$

When the temperature of the droplet reaches the boiling point, the droplet remains at its boiling temperature. A boiling rate equation is applied to calculate the mass transfer as follows (Ref 15)

$$\frac{d(d_d)}{dt} = \frac{4k_f(1 + 0.23\sqrt{Re_d})}{\rho_d c_f d_d}\ln\left[1 + \frac{c_f(T_f - T_d)}{h_{fg}}\right]. \qquad \text{(Eq 10)}$$

In the forgoing equations subscript f and d denote fluid and droplet, respectively.

When all the solvent goes away, the model assumes that the solution droplet forms a solid particle. The diameter of the particle is calculated according to the mass fraction or volume fraction of the solute in the solution. Then, the heating of the particle can be calculated by

Eq (8). When the particle reaches its melting point, its temperature is set to the melting point, and no mass transfer is calculated.

2.2 Injection Modes

The solution is injected into the plasma jet in SPPS either by a liquid stream injection or a gas-blast injection (Fig. 2). For the liquid stream injection, the liquid in a container is pressed and accelerated through a nozzle to form a liquid jet. If adding constant pressure pulses in the container, the jet may break up into mono-dispersed droplets before it interacts with the plasma jet (Fig. 2a), and then experiences the secondary breakup when the droplets penetrate into the plasma jet. It is also possible that the jet undergoes the primary breakup or maintains as a jet before it penetrates into the plasma jet (Fig. 2b). It depends on the geometry of the nozzle, the injection pressure, surrounding flow conditions, and the properties of the liquid. For the gas-blast injection, the liquid is atomized into droplets by a gas and injected into the plasma jet followed by the secondary breakups (Fig. 2c). The size distribution of the gas-blast injection depends on the nozzle geometry, the gas velocity, the mass flow rate, and the liquid properties.

2.2.1 Modeling the Liquid Stream Injection. According to the analysis in previous text, the liquid stream injection is treated as two different cases: the liquid jet undergoes the primary breakup before it interacts with the plasma jet (case 1), and the liquid jet breaks up into mono-dispersed droplets or maintains as a jet (case 2) before it penetrates into the plasma jet. The models for the two cases are described as follows:

Case 1. The physical processes involving in the liquid stream injection include the internal nozzle flow and the external atomization, which is very complex. To simplify the model, it is assumed that the liquid completely fills the orifice. The injection velocity of the stream can be calculated based on the conservation of mass and the assumption of a uniform injection velocity:

$$u_l = \frac{m_d}{\rho_d A}. \quad \text{(Eq 11)}$$

The spray angle is determined by the following correlation (Ref 16):

$$\theta = 2\tan^{-1}\left[\frac{4\pi}{C_A}\sqrt{\frac{\rho_g}{\rho_d}}\frac{\sqrt{3}}{6}\right], \quad \text{(Eq 12)}$$

where $C_A = 3 + (L/3.6d)$.

The Sauter mean diameter and the most probable droplet diameter of the droplets are calculated by (Ref 17):

$$d_{32} = 16.63 d We_d^{-0.74}, \quad \text{(Eq 13)}$$

$$d_0 = 1.2726 d_{32}(1-s)^s, \quad \text{(Eq 14)}$$

where $s = 0.286$ (Ref 18). Then the droplet diameter distribution is determined by Rosin-Rammler distribution. During the trajectory and heating of the droplets, TAB breakup model is used to model the secondary breakup of the droplets (Ref 8). TAB model is based on an analogy between an oscillating and distorting droplet and a spring-mass system. It is applicable to low-Weber-number ($We < 100$) liquid injections into a standard atmosphere. Although the absolute velocity of the droplet is high in SPPS, the relative velocity between the jet and the droplet is low during the trajectory (meanwhile at the beginning of the trajectory, it could be high), and the *We* numbers of droplets are low too, the TAB model is applicable for the operating conditions used in this study.

Case 2. For the case that the liquid jet breaks up into mono-dispersed droplets or maintains as a jet before it interacts with the plasma jet, a train of mono-dispersed, whose diameter is equal to the diameter of the orifice, is used to represent the liquid jet. The spray angle is zero, and the injection velocity can be determined by Eq (11). The breakup of the jet (or the mono-dispersed droplet) is then calculated by Reitz wave breakup model. The Reitz wave breakup model determines how and when droplets breakup by calculating the wavelength and the growth rate of the fastest growing disturbances on the surface of a droplet (or a jet) due to aerodynamic instabilities. The wavelength and growth rate are given as follows (Ref 19):

$$\Lambda = \frac{9.02 r_d\left(1+0.45\sqrt{\mathrm{Oh}}\right)\left(1+0.4\mathrm{Ta}^{0.7}\right)}{\left(1+0.865 We_g^{1.67}\right)^{0.6}}, \quad \text{(Eq 15)}$$

$$\Omega = \frac{0.34 + 0.385 We_g^{1.5}}{(1+\mathrm{Oh})(1+1.4\mathrm{Ta}^{0.6})} \cdot \frac{\sigma_d}{\rho_d r_d^3}, \quad \text{(Eq 16)}$$

where $\mathrm{Oh} = \sqrt{\frac{We_d}{Re_d}}$, $\mathrm{Ta} = \mathrm{Oh}\sqrt{We_g}$.

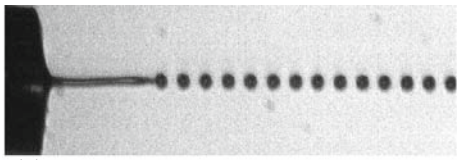

(a) The mono-droplets injection.

(b) The liquid jet injection.

(c) The gas-blast injection.

Fig. 2 Illustration of injection modes. (a) The mono-droplets injection; (b) the liquid jet injection; and (c) the gas-blast injection

The breakup time is given by:

$$\tau_b = \frac{3.788 C_1 r_d}{\Lambda\Omega}, \quad \text{(Eq 17)}$$

C_1 is an adjustable constant and dependent on the characteristics of the injector.

The radius of the droplets is determined by the relationship between the calculated wavelength and the original droplet radius. If the droplet radius is smaller than some fraction of the breakup wavelength, the droplets are assumed to be breaking off from the liquid core in the center of the spray. In this case, the new droplet radius is allowed to have a radius larger than the nozzle radius. If the droplet radius is larger than some fraction of the breakup wavelength, the disturbance results in new droplets being shed from the original droplets. The radius of the new droplets is assumed proportional to the calculated wavelength, given by:

$$r_d^{shed} = C_2 \Lambda, \quad \text{(Eq 18)}$$

C_2 is set to 0.61 in this model (Ref 19). Then the droplet radius is given by:

$$r_d^{new} = \frac{\tau_b r_d + dt(C_2\Lambda)}{\tau_b + dt}, \quad \text{(Eq 19)}$$

where dt is the current time step.

2.2.2 Gas-blast Injection (Case 3). The physical process involving in the gas-blast injection is more complex than that of the liquid stream injection since a gas stream is introduced. Generally speaking, the gas stream can accelerate the breakup of the liquid and disperse the droplets quickly, thus fine droplets can be produced. The atomization mechanism of this process is not completely understood though efforts have been made to simulate this process (Ref 20). To avoid complex coupling calculation, a droplet size distribution is chosen based on the experiment observation to represent the gas-blast injection, and the effect of the atomization gas on the plasma jet is ignored. However, it must be noted that the transverse injection of the atomization gas may cause appreciable 3D effects. This will cause the trajectory and heating of the droplets different from those neglecting the effect of the atomization gas. After the injection of the droplets, TAB breakup model is used to model the secondary breakup of the droplets (Ref 8).

2.2.3 Initial and Boundary Conditions. The initial temperature, mass flow rate of the solution, the diameter, and the position of the nozzle or droplets for all injection modes are specified. During the calculation, if a droplet hits a wall or crosses the computational boundaries, trajectory calculations are terminated.

3. Results and Discussion

The governing equations of the plasma jet are solved using Fluent CFD code (Ref 21) with temperature-dependent thermodynamic and transport properties. The models of the injection modes are implemented into the plasma jet model. The method used to solve the injection models is based on the ideas of Monte Carlo method and of discrete particle method. The diameter of the torch exit is 7.8 mm. The solution mass flow rate is 0.0003 kg/s. The solvent is water. The final product of the solute is $(La_{0.85}Sr_{0.15})MnO_3$ (LSM) (specific mass: 6570 kg/m^3, specific heat 573 J/kg K, thermal conductivity 4 W/m K, melting temperature 2153 K). The maximum axial velocity and temperature on the centerline at the torch exit are $u_m = 1090$ m/s and $T_m = 13490$ K, respectively. Ar flow rate is 62 slpm and H_2 flow rate is 2 slpm. The plasma gas mass flow rate is 0.0018 kg/s. The jet impinges onto a substrate locates 80 mm away from the torch exit. The injector locates at the position (0.004 m, 0°, 0.01 m) as shown in Fig. 1.

3.1 Plasma Jet Fields

Figures 3-5 show the temperature (Fig. 3), velocity magnitude (Fig. 4), and argon mass fraction distributions (Fig. 5) on the RZ plane of the jet. The predicted fields are used as the base to perform the following calculations.

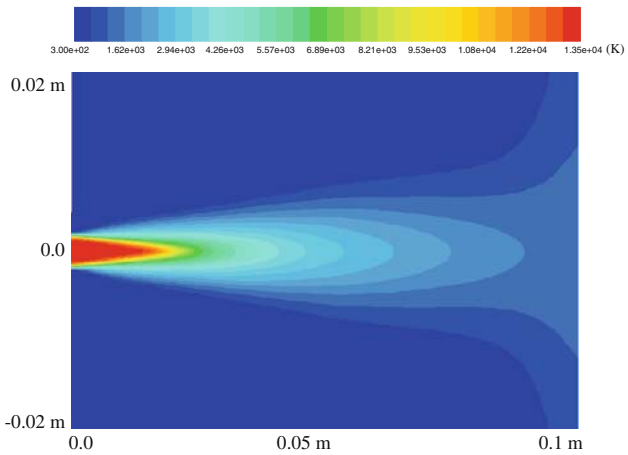

Fig. 3 Temperature distribution of the jet on RZ plane

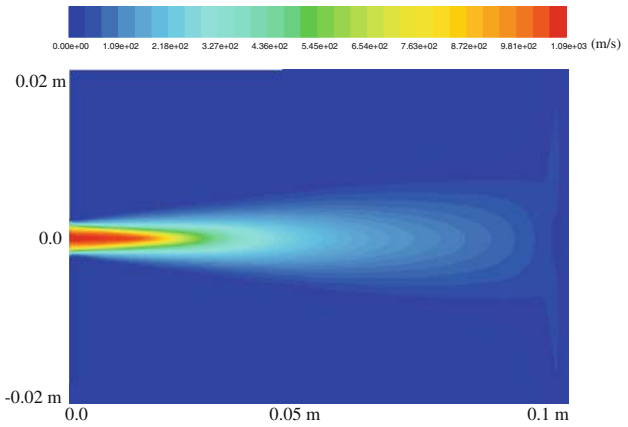

Fig. 4 Velocity magnitude distribution of the jet on RZ plane

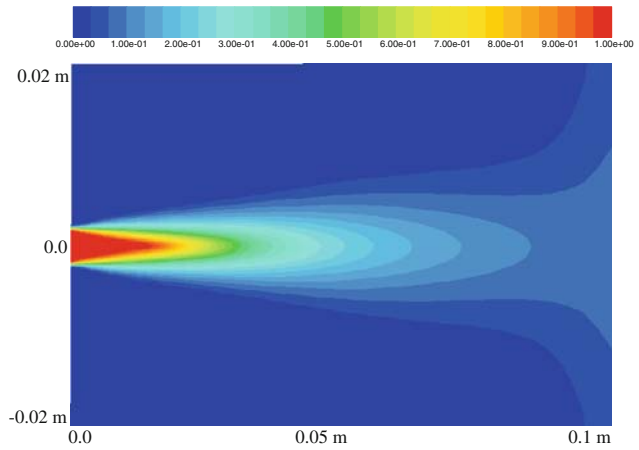

Fig. 5 Argon mass fraction distribution of the jet on *RZ* plane

3.2 Influence of Injection Modes

In the calculations, an injection nozzle with an exit diameter of 100 μm is used for case 1. A train of uniform droplets with diameter of 100 μm is used for case 2. For the gas-blast injection nozzle (case 3), initial droplet size distribution is chosen based on the experiment observation. The minimum droplet diameter is 10 μm and the maximum droplet diameter is set to 60 μm. The injection velocity is 20-75 m/s. The initial temperature is 300 K. Figure 6 shows the droplet/particle size distribution on the cross section at $Z = 80$ mm for different injection modes. The results show that the finest droplets were collected for case 3. Droplets with diameter above 20 μm present both in case 1 and case 2, but the portion of small droplets in case 1 is greater than that of case 2. For case 1, the liquid stream experiences the primary breakup, most of the atomized droplets are then injected into the plasma jet, where secondary breakup may take place as the aerodynamic force working on the droplet exceed the surface tension force and internal viscous force of the droplet. Since atomized droplets disperse in a spray angle, some of them will not penetrate into the jet core area. These droplets are not effectively heated and may not experience secondary breakup, which results in bigger droplets downstream. For case 2, the stream begins the primary breakup only when it interacts with the plasma jet. The relative high momentum of the stream makes it penetrate further than that of the droplets in case 1. That means the atomized droplets can pass through the hot core area of the plasma jet. As a result, the solvent evaporates very quickly and the droplet may not experience the secondary breakup before it becomes the solid particle. Therefore, the bigger solid particles are produced, and then heated and accelerated to impact on the substrate.

It can be seen from Fig. 7 that the predicted droplet/particle temperature distributions for the three cases show that, though the droplet/particle sizes are bigger than that of the other two cases, the droplet/particles are effectively heated in case 2. The temperature of the majority of the

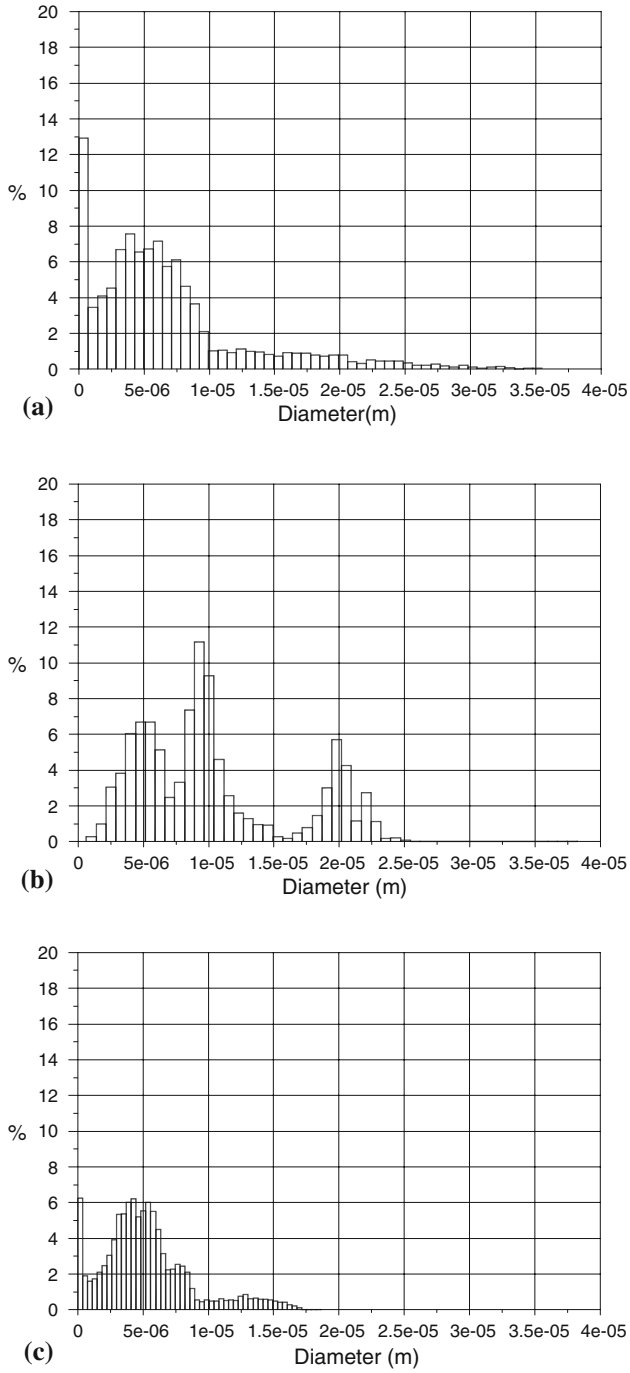

Fig. 6 Droplet/particle size distribution at $Z = 80$ mm. (a) Case 1; (b) Case 2; and (c) Case 3

particles reaches its melting point. Only a very small portion of particles arrives at the substrate in the state of a liquid. Case 3 has the largest portion of the particles that are solution droplets. It may come from the fact that for case 3 fine droplets are obtained after the primary breakup, some of them may not gain enough momentum to penetrate into the hot area of the plasma jet. It can be seen from the particles position distribution on

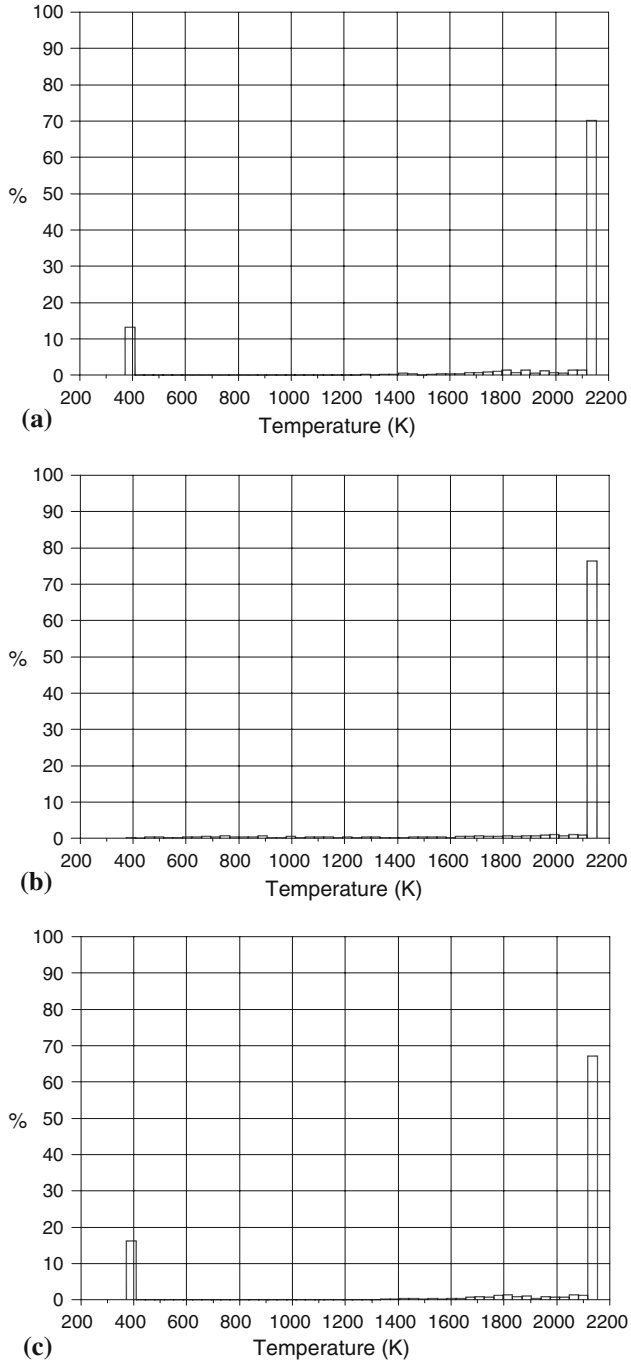

Fig. 7 Droplet/particle temperature distribution at $Z = 80$ mm. (a) Case 1; (b) Case 2; and (c) Case 3

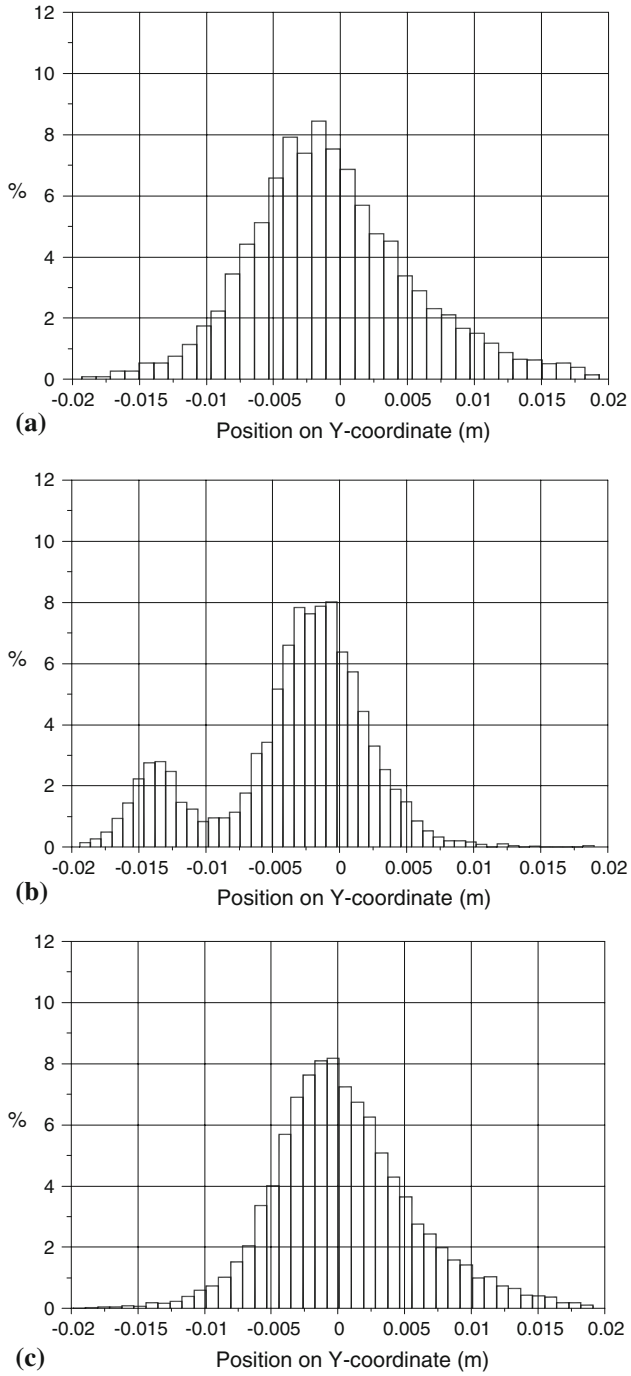

Fig. 8 Droplet/particle position distribution at $Z = 80$ mm. (a) Case 1; (b) Case 2; and (c) Case 3

Y-coordinate of the substrate (Fig. 8). For case 1 and case 3, the droplet/particle distribution on *Y*-coordinate only has a slight offset from the centerline, while in case 2 the offset from centerline is evident. As analyzed in previous text, this is because the droplets generated in case 2 have higher momentum and are not dispersed in trajectory axis before it interacts with the plasma jet, which makes them penetrate further and pass through the jet core area.

4. Conclusions

The solution is injected into the plasma jet in the solution precursor plasma spraying either by a liquid stream injection or a gas-blast injection. A numerical study is performed in this article to investigate the effect of the injection modes on the trajectory and heating of the solution in SPPS. Three cases are considered: the liquid

stream injection with primary breakup, the liquid jet or mono-dispersed droplets, and the gas-blast injection. The particle/droplet size, temperature, and position distributions on the substrate are predicted for different injection modes. The results show that the gas-blast injection can produce smaller droplets than the stream injection mode, while the liquid jet mode allows injecting the solution droplets into the hot core area of the plasma jet, which makes the droplets heated effectively. The liquid stream injection mode with primary breakup performs in between of the two modes. It should be noted that neglecting the effects of arc voltage fluctuation and the atomization gas on the plasma jet limits the application of this model, and it should be included in further study so that the predictions of the model become more realistic.

Acknowledgments

This work is supported by the Natural Science Foundation of China (No. 50706027), the Innovation Program of Shanghai Municipal Education Commission (No. 09YZ206), and the Shanghai Leading Academic Discipline Project (No. J50501).

References

1. J. Karthikeyan, C.C. Berndt, S. Reddy, J.Y. Wang, A.H. King, and H. Herman, Nanomaterial Deposits Formed by DC Plasma Spraying of Liquid Feedstocks, *J. Am. Ceram. Soc.*, 1998, **81**(1), p 121-128
2. N.P. Padture, K.W. Schlichting, T. Bhatia, A. Ozturk, B.M. Cetegen, E.H. Jordan, and M. Gell, Towards Durable Thermal Barrier Coatings with Novel Microstructures Deposited by Solution-precursor Plasma Spray, *Acta Mater.*, 2001, **49**(12), p 2251-2257
3. L. Xie, X. Ma, A. Ozturk, E.H. Jordan, N.P. Padture, B.M. Cetegen, D. Xiao, and M. Gell, Processing Parameter Effects on Solution Precursor Plasma Spray Process Spray Patterns, *Surf. Coat. Technol.*, 2004, **183**(1), p 51-61
4. Y. Shan, Y. Wang, and T. Coyle, Analysis of the Deposition Mechanism in the Solution Precursor Plasma Spraying using Numerically Predicted Particle Conditions, Thermal Spray Crossing Borders, *Proceedings of ITSC2008*, E. Lugscheider, Ed., DVS-Verlag, Düsseldorf, Germany, 2008, CD-ROM
5. Y. Shan, T. Coyle, and J. Mostaghimi, 3D Modeling of Transport Phenomena and the Injection of the Solution Droplets in the Solution Precursor Plasma Spraying, *J. Therm. Spray Tech.*, 2007, **16**(5-6), p 736-743
6. J. Fazilleau, C. Delbos, V. Rat, J.F. Coudert, P. Fauchais, and B. Pateyron, Phenomena Involved in Suspension Plasma Spraying, Part 1: Suspension Injection and Behavior, *Plasma. Chem. Plasma Process.*, 2006, **26**(2), p 371-391
7. S. Basu, E.H. Jordan, and B.M. Cetegen, Fluid Mechanics and Heat Transfer of Liquid Precursor Droplets Injected into High-temperature Plasmas, *J. Therm. Spray Tech.*, 2008, **17**(1), p 60-72
8. Y. Shan, T. Coyle, and J. Mostaghimi, Numerical Simulation of Droplet Breakup and Collision in the Solution Precursor Plasma Spraying, *J. Therm. Spray Tech.*, 2007, **16**(5-6), p 698-704
9. L. Xie, X. Ma, E. Jordan, N. Padture, D. Xiao, and M. Gell, Identification of Coating Deposition Mechanisms in the Solution-precursor Plasma-spray Process Using Model Spray Experiment, *Mater. Sci. Eng. A*, 2003, **362**, p 204-212
10. L. Xie, E.H. Jordan, N.P. Padture, and M. Gell, Phase and Micro-structural Stability of Solution Precursor Plasma Sprayed Thermal Barrier Coatings, *Mater. Sci. Eng. A*, 2004, **381**(1-2), p 189-195
11. Y. Wang and T. Coyle, Solution Precursor Plasma Spray of Nickel-Yittia Stabilized Zirconia Anodes for Solid Oxide Fuel Cell Application, *J. Therm. Spray Tech.*, 2007, **16**(5-6), p 898-904
12. C. Marchand, C. Chazelas, G. Mariaux, and A. Vardelle, Liquid Precursor Plasma Spraying: Modeling the Interactions Between the Transient Plasma Jet and the Droplets, *J. Therm. Spray Tech.*, 2007, **16**(5-6), p 705-712
13. P. Fauchais, R. Etchart-Salas, V. Rat, J.F. Coudert, N. Caron, and K. Wittmann-Ténèze, Parameters Controlling Liquid Plasma Spraying: Solutions, Sols, or Suspensions, *J. Therm. Spray Tech.*, 2008, **17**(1), p 31-59
14. S.A. Morsi and A.J. Alexander, An Investigation of Particle Trajectories in Two-phase Flow Systems, *J. Fluid Mech.*, 1972, **55**, p 193-208
15. K.K.Y. Kuo, *Principles of Combustion*, John Wiley and Sons, New York, 1986
16. W. Ranz, Some Experiments on Orifice Sprays, *Can. J. Chem. Eng.*, 1958, **36**, p 175-191
17. P. Wu, L. Tseng, and G. Faeth, Primary Breakup in Gas/Liquid Mixing Layers for Turbulent Liquids, *Atomiz. Sprays*, 1995, **2**, p 295-317
18. A.H. Lefebvre, *Atomization and Sprays*, Hemisphere Publishing Corporation, New York, 1989
19. R. Reitz, Mechanisms of Atomization Processes in High-pressure Vaporizing Sprays, *Atomiz. Spray Technol.*, 1987, **3**, p 309-337
20. D. Schmidt, I. Nouar, P. Senecal, C. Rutland, J. Martin, and R. Reitz, *Pressure Swirl Atomization in the Near Field*, SAE Paper 01-0496, SAE, 1999
21. Fluent Inc., Fluent V6.2manual, Lebanon, NH, USA, 2005